Soft Matter

Cite this: *Soft Matter*, 2011, **7**, 4198

www.rsc.org/softmatter

PAPER

Self-assembled structures in rod-coil block copolymers with hydrogen-bonded amphiphiles†

Han-Sheng Sun,[a] Chia-Hao Lee,[a] Chia-Sheng Lai,[c] Hsin-Lung Chen,[c] Shih-Huang Tung*[a] and Wen-Chang Chen*[ab]

Received 28th November 2010, Accepted 9th February 2011
DOI: 10.1039/c0sm01385d

We report the synthesis and the self-assembled morphologies of a series of new rod-coil diblock copolymers, poly[2,7-(9,9-dihexylfluorene)]-*b*-poly(4-vinylpyridine) (PF-*b*-P4VP). The rod-coil diblock copolymers were synthesized *via* Suzuki coupling reaction and living anionic polymerization. Probing by transmission electron microscopy, small-angle X-ray scattering and atomic force microscopy, we found that the microphase separation varies from lamellar to cylindrical and then to spherical, depending on the length of P4VP blocks. The P4VP coil blocks were further hydrogen-bonded with 3-pentadecylphenol (PDP) to form rod-comb block copolymers. Similar to conventional coil-coil block copolymers-based supramolecules, the incorporation of PDP transforms the morphologies from lamellar to cylindrical or from cylindrical to spherical due to the increase of volume fraction of P4VP(PDP) comb blocks. The strategy described here can be used to tune the self-assembled structures of rod-coil block copolymers.

1. Introduction

Rod-coil block copolymers have been an important class of nanomaterials, not only because of their potential for the biological and optoelectronic applications but also the richness of phase behaviors that fascinate many nanotechnologists.[1–3] In rod-coil block copolymers, flexible coil-like chains are covalently bonded to one or more blocks with rod-like chains due to π-conjugation, helical secondary structures, or aromatic mesogenic groups along the backbone. The incorporation of rigid rod-like chains into the block copolymers results in asymmetric chain conformations. Their self-assembly behaviors are thus very different from those of conventional coil-coil block copolymers. In addition to the classical theories for the microphase separation of the rod and coil components, an important thermodynamic factor that needs to be taken into account is the strong tendency of rods to stack and align due to the strong interaction between rods and the large excluded volume of long rigid rods, which in fact usually dominates the microphase separation. Moreover, the anisotropic alignments of rigid rods may lead to liquid crystalline or crystalline phases,[4–8] further increasing the complexity of phase behaviors. A great number of efforts, experimental or theoretical, have been made to unravel the systems of rod-coil block copolymers and a variety of nanostructures have been reported in solutions, melts, and thin films.[1–3] However, the results are usually interpreted on a case-by-case basis and a universal theoretical framework for explaining the phase behavior is still under development.[9]

Conjugated polymers are unique organic materials that possess electronically and optically active properties due to the delocalization of π-electrons. The π-interaction also imparts rigidity thereby giving rise to a rod-like chain. In addition to chemical architectures, the electrical and optical properties of conjugated polymers are highly dependent on structures, such as the interchain distance and the chain orientation.[10] Thus, manipulation of the structure is important for conjugated polymers to function efficiently with desired properties. One promising way to do so is incorporation of flexible chains into conjugated polymers to form rod-coil block copolymers in which the aggregation sizes and stack ordering of conjugated blocks can be tailored by the flexible blocks.[11] Various conjugated moieties of π-conjugated rod-coil block copolymers have been reported,[1–3] among which polyfluorene (PF) is widely investigated for optoelectronic applications due to its good thermal and chemical stability, fluorescence quantum yields, and charge carrier mobility.[12–14] Several polyfluorene-based rod-coil block copolymers have been reported and most of the studies have focused on the self-assembled structures in solutions or the dependence of optoelectronic properties on the other blocks.[15–20]

The concept of supramolecules has been increasingly adopted in the nanotechnology of polymeric materials since it can prevent

[a]*Institute of Polymer Science and Engineering, National Taiwan University, Taipei, 10617, Taiwan. E-mail: shtung@ntu.edu.tw; chenwc@ntu.edu.tw*
[b]*Department of Chemical Engineering, National Taiwan University, Taipei, 10617, Taiwan*
[c]*Department of Chemical Engineering, National Tsing Hua University, Hsin-Chu, 30013, Taiwan*

† Electronic supplementary information (ESI) available: the GPC data of PF_9-*b*-$P4VP_{22}$ and the morphologies of more PF-*b*-P4VP copolymers and PF-*b*-P4VP(PDP) supramolecules. See DOI: 10.1039/c0sm01385d

the complexity of synthesizing new polymers and can create functional materials with reversible properties.[21–23] The incorporation of small molecules which graft onto backbone of polymers *via* secondary bonds results in a comb-like structure. In block copolymer system, the added small molecules associated with one of the blocks can alter the volume fractions of blocks and a morphological transition occurs. Furthermore, the small molecule itself can assemble into lamellae in one of the microdomains, forming hierarchical structure-within-structure morphologies.[24] More interestingly, in coil-coil block copolymer thin films, the graft effects can be used to manipulate the orientation of microdomains with respect to the surface, which provides a facile route to control the nanostructures and properties of thin films.[25–28] Poly(4-vinylpyridine) (P4VP) is commonly used to study the self-assembly of block copolymer-based supramolecules since its pyridine groups can easily form hydrogen bonds or ionic bonds with other molecules. Mezzenga and coworkers have reported the morphology of P4VP-based rod-coil block copolymers, poly(diethylhexyloxy-*p*-phenylenevinylene)-*b*-P4VP,[29] and the use of supramolecules of poly(3-hexylthiophene)-*b*-poly(4-vinylpyridine) with PCBM for photovoltaic applications.[30] The microphase separation of rod-comb supramolecules, however, has not yet been systematically explored.

In this study, we synthesized poly[2,7-(9,9-dihexylfluorene)]-*b*-poly(4-vinylpyridine) (PF-*b*-P4VP) rod-coil diblock copolymers by combining Suzuki coupling reaction and living anionic polymerization. The PF blocks possess optoelectronic functionality while P4VP blocks are the media used to manipulate the nanostructures. We then prepared the rod-comb supramolecules by mixing PF-*b*-P4VP and 3-pentadecylphenol (PDP), an amphiphilic molecule which associates with 4VP *via* hydrogen bonds. The morphologies of PF-*b*-P4VP and its supramolecules in bulk states and thin films were studied by transmission electron microscopy (TEM), small-angle X-ray scattering (SAXS), grazing incidence small-angle X-ray scattering (GISAXS) and atomic force microscopy (AFM). A series of morphologies, lamellar, cylindrical, and spherical, could be obtained by varying the lengths of P4VP blocks and the amount of added PDP.

2. Experimental section

Materials

9,9-Dihexyl-2,7-dibromofluorene (97%, Aldrich), triisopropyl borate (>98%, Aldrich), tetrakis(triphenylphosphine) palladium(0) ($Pd(PPh_3)_4$, 99%, Aldrich), potassium carbonate (K_2CO_3, >99%, Acros), 4-bromostyrene (98%, Aldrich), phenylboronic acid (97%, Aldrich), n-butyllithium (*n*-BuLi, 2.5 M in hexane, Chemetall), *sec*-butyllithium (*sec*-BuLi, 1.3 M in cyclohexane/hexane (92/8), Chemetall), Aliquat® 336 (trioctylmethylammonium chloride, Aldrich), hydrochloric acid (HCl, 37%, Scharlab S.L.), and 3-pentadecylphenol (PDP, 90%, Aldrich) were used without further purification. Toluene (anhydrous, Acros), hexane (Mallinckrodt Chemical, Inc.), methyl alcohol (MeOH, >99%, Aldrich), chloroform (Mallinckrodt Chemical, Inc.) were used as received. 4-Vinyl pyridine (4VP, 95%, Acros) was distillated from CaH_2 powder (93%, Acros) and dibutylmagnesium (1.0 M solution in heptane, Aldrich) under reduced pressure. Tetrahydrofuran (THF, 99.9%, Acros) was distillated from sodium (30∼35 wt % dispersion in paraffin wax, Aldrich) and benzophenone (>99%, Aldrich) mixture.

Synthesis of poly[2,7-(9,9-dihexylfluorene)]-*block*-poly(4-vinylpyridine)

The synthesis route is shown in Scheme 1. We first synthesized poly[2,7-(9,9-dihexylfluorene)] macroinitiator (PF-Vinyl) (**3**). The procedure is described as follows: 2-bromo-9,9-di-*n*-hexylfluoreneboronic (**2**) was prepared by monolithiation of 9,9-dihexyl-2,7-dibromofluorene (**1**) with 1.1 equimolar amounts of *n*-butyllithium followed by boronation with triisopropyl borate at −78 °C (yield: 52%).[16] Poly[2,7-(9,9-dihexylfluorene)] macroinitiator was synthesized by modified Suzuki coupling.[31] 1.50 g (3.29 mmol) 2-bromo-9,9-di-*n*-hexylfluoreneboronic (**2**), 57.5 μl (0.53 mmol) 4-bromostyrene, 81.1 mg (0.070 mmol) $Pd(PPh_3)_4$, 15 ml K_2CO_3 aqueous solution (2.0 M), 20 ml toluene, and 5 drops Aliquat® 336 were mixed. After stirred vigorously at 85 °C for 24 h, a solution of 1.50 g (12.31 mmol) phenylboric acid, 26 mg (0.022 mmol) $Pd(PPh_3)_4$, and 15 ml THF was added and reacted for 12 h to cap the bromo-side. The resulting mixture was cooled to room temperature, and poured into 700 ml methanol for the polymer to precipitate. The collected solid was re-dissolved in 5 ml of THF, re-precipitated twice in 700 ml of methanol, and then dried under vacuum at 50 °C for 24 h. 986.8 mg of green powder PF-vinyl (**3**) was obtained (yield: 66%). The number-average molecular weight (M_n) from GPC measurements (THF as the carrier solvent) was 3002 g mol^{-1} and the polydispersity index (PDI) was 1.87. The degree of polymerization was also determined by the ratio of fluorene units to the vinyl end group calculated from ^1H NMR spectrum and the value of 8.8 is consistent with the molecular weight determined by GPC. The degree of polymerization was thus estimated to be 9. ^1H NMR ($CDCl_3$): δ (ppm) = 0.76–0.85 (m, 3H, -$(CH_2)_5C\underline{H}_3$), 1.11–1.26 (m, 8H, -$CH_2(C\underline{H}_2)_4CH_3$), 2.08–2.17 (m, 2H, -$C\underline{H}_2(CH_2)_4CH_3$), 5.29 and 5.81 (2d, 2H, $C\underline{H}_2$=), 6.70–6.85 (m, 1H, C<u>H</u>=), 7.38–7.84 (m, 15H, protons on fluorene and phenyl end groups).

We then synthesized poly[2,7-(9,9-dihexylfluorene)]-*block*-poly(4-vinylpyridine) (**4**) by living anionic polymerization, similar to that reported in the literature.[32] 102.4 mg (0.032 mmol) PF_9-vinyl macroinitiator was placed in a 250 ml reaction flask and then evacuated to 10∼20 mtorr for 3 h in order to remove the residual solvent and undesired moisture. 100 ml purified THF was transferred into the reactor, stirred for 10 min and cooled to −78 °C. Excess *sec*-butyllithium was used as initiator and added to the well-stirred solution using a syringe. The color of the solution was changed from green to black immediately, indicating that the PF macroinitiators were initiated. The reaction flask was warmed up to room temperature for 1 h for the excess *sec*-butyllithium to react with THF to form ethylene and a lithium salt. The solution was cooled to −78 °C again. The purified 4-vinylpyridine monomers were then injected into the reaction flask quickly and polymerized for 1 h. Finally, the living anionic polymerization was terminated by an aliquot of methanol and then precipitated in hexane. The PF-*b*-P4VP rod-coil diblock copolymer was collected and dried under vacuum at

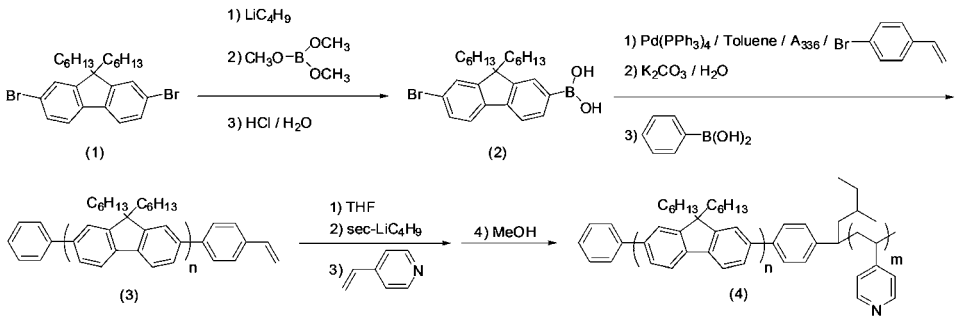

Scheme 1 The synthetic route of PF-*b*-P4VP linear rod-coil diblock copolymers.

80 °C for 24 h (yield: 95%). The molecular weights of P4VP blocks in copolymers were determined based on the copolymer compositions measured by ^{1}H NMR and the molecular weight of PF macroinitiators, which are listed in Table 1. Since PF-*b*-P4VPs are unable to completely dissolve in any solvents commonly used for GPC measurements, the determination of PDIs is difficult. We could only obtain the PDI of PF_9-*b*-$P4VP_{22}$, ~1.78, which were measured in DMF. Since the PDIs of the P4VP homopolymers we synthesized using living anionic polymerization were ~1.20, PDI values between 1.20 and 1.87 should be reasonably expected for PF_9-based copolymers. The GPC data of PF_9-*b*-$P4VP_{22}$ and a detailed discussion of GPC measurements are included in the ESI.† ^{1}H NMR ($CDCl_3$): δ (ppm) = 0.77–0.84 (m, 3H, -$(CH_2)_5C\underline{H}_3$), 1.13 (broad, 8H, -$CH_2(C\underline{H}_2)_4CH_3$), 2.11 (broad, 2H, -$C\underline{H}_2(CH_2)_4CH_3$), 6.27–6.43 and 8.22–8.40 (broad, 2H, protons on pyridine groups), 7.37–7.83 (m, 15H, protons on fluorene and phenyl end groups).

Sample preparation

The rod-coil diblock copolymer, PF-*b*-P4VP, was first dried in vacuum oven for 1 day and dissolved in chloroform to form 1–2% (w/v) stock solutions. Bulk samples were prepared by placing the polymer solutions in 1 ml Teflon beakers, and then the solvents were evaporated at room temperature for several days. Samples were further dried and annealed under vacuum at 150 °C for 48 h. Thin films were prepared by spin-coating the solutions onto silicon wafers at spinning speed 3000 rpm. The solutions were diluted in order to obtain desired film thicknesses. Thin films were then solvent-annealed, which was conducted by placing films inside an inverted dish (170 mm D × 90 mm H) together with a beaker of 40 ml of chloroform at room temperature for 2 days. Film thicknesses were measured using a Filmetrics F20 interferometer or a Surfcorder ET3000 profilometer (Kosaka Lab). For the preparation of PF-*b*-P4VP(PDP) complexes, the desired amount of PDP was dissolved in chloroform. The PF-*b*-P4VP solutions were then added dropwise to the PDP solution, followed by stirring for at least 3 days at room temperature to form stock solutions. The bulk samples were prepared following the procedures for PF-*b*-P4VP bulk samples but annealed at 105 °C for 48 h. Annealing at lower temperature is to prevent the PDPs from evaporation. The thin film samples were prepared following the procedures described above.

Characterization

The molecular weight distribution of the prepared polymers was determined by the gel permeation chromatography (GPC) using a Lab Alliance RI2000 instrument equipped with MIXED-C and D columns and a refractive index detector. THF or DMF was used as the carrier solvent at flow rate 1 ml min^{-1} at 40 °C and calibrated with polystyrene standards. The ^{1}H NMR measurements were conducted on a Bruker Avance DRX 500 MHz FT-NMR system. Deuterated chloroform with standard tetramethylsilane (TMS) was used. Thermogravimetric analysis (TGA) was performed on a PerkinElmer Pyris 7 TGA. 3~5 mg powder samples were heated under flowing nitrogen (flow rate 20 cm^3 min^{-1}) at a heating rate of 20 °C min^{-1} from room temperature to 800 °C. The glass transition temperatures were determined using a TA Instrument DSC Q100 at a heating rate of 5 °C min^{-1} from −30 °C to 250 °C. FT-IR spectra were recorded at room temperature using a Jasco Model FTIR 410 spectrophotometer. Samples were cast on KBr pellets and scanned 64 times with resolution 8 cm^{-1}.

Samples prepared for transmission electron microscopy (TEM) were embedded in resin and cured at 60 °C overnight and then were microtomed to sections with thickness ~80 nm. The thin sections were exposed to either RuO_4 or iodine vapor that selectively stain the PF or P4VP block, respectively, to enhance the contrast. TEM images were collected on a Joel JEM-1230 transmission electron microscope at an accelerating voltage of

Table 1 Characteristics of PF-*b*-P4VP rod-coil block copolymers

Sample	$M_{n,PF}$[b] (g mol^{-1})	$M_{n,P4VP}$[b] (g mol^{-1})	f_{4VP}[c]	T_g (°C)	Morphology
PF_9-*b*-$P4VP_{22}$[a]	3120	2310	0.42	84	lamella
PF_9-*b*-$P4VP_{92}$	3120	9730	0.76	145	cylinder
PF_9-*b*-$P4VP_{231}$	3120	24340	0.89	147	sphere

[a] subscripts denote degree of polymerization. [b] molecular weight determined by NMR. [c] weight fraction of P4VP.

100 kV. Atomic force microscopy (AFM) imaging was performed on a MultiMode AFM system with a Nanoscope 3D controller (Digital Instruments) in tapping mode. The spring constant of the silicon cantilevers (Nanosensor PPP-SEIHR) was 15 N m^{-1} and the resonant frequency was 130 kHz.

Small-angle X-ray scattering (SAXS) measurements of pure PF-*b*-P4VPs were conducted on a Bruker NANOSTAR SAXS apparatus, equipped with a 3.0 kW X-ray generator operated at 40 kV × 35 mA and a two-dimensional position-sensitive proportional counter. The Cu-Kα line with wavelength $\lambda = 1.54$ Å was used. SAXS data of PF-*b*-P4VP(PDP) complexes were collected on beamline BL23A1 in the National Synchrotron Radiation Research Center (NSRRC), Taiwan. A monochromatic beam of $\lambda = 0.887$ Å was used.[33] The scattering intensity profiles were reported as the plots of the scattering intensity (I) *vs.* the scattering vector q, where $q = (4\pi/\lambda)\sin(\theta/2)$, θ is the scattering angle. Grazing incidence small-angle X-ray scattering (GISAXS) measurements were also conducted on beamline BL23A1 in NSRRC, with a wavelength of 0.887 Å at an incident angle of 0.2°. The scattering profiles were collected on a Mar-CCD with a diameter of 165 mm.[33]

3. Results and discussion

Chemical structures and thermal properties of PF-*b*-P4VP

The synthesized rod-coil block copolymers with PF of 9 repeat units and varying P4VP lengths are listed in Table 1. The chemical structures of the synthesized polymers were confirmed by ^{1}H NMR spectrum. Fig. 1a shows the ^{1}H NMR spectrum of PF macroinitiator in *d*-chloroform. The proton resonance peaks at 0.76–0.85, 1.11–1.26 and 2.08–2.17 ppm are assigned to the methyl and methylene of the alkyl group on the PF moiety, respectively. The signals between 7.26–7.84 ppm are attributed to the fluorene aromatic protons and phenyl end group. The proton signals on the vinyl moiety of macroinitiator are clearly observed at 5.29, 5.81 and 6.70–6.85 ppm, indicating the successful incorporation of the end-capper 4-bromostyrene. After polymerization, the proton peaks of vinyl group of the PF macroinitiator at 5.29 and 5.81 ppm entirely disappear and the proton signals of the pyridine groups at 6.38–6.86 and 8.36–8.44 ppm are observed in PF-*b*-P4VP rod-coil block copolymer, as shown Fig. 1b. These results confirm the successful synthesis of the PF macroinitiator and block copolymer PF-*b*-P4VP.

The thermal properties of the synthesized polymers were measured by TGA and DSC. Fig. 2a shows the thermal decomposition temperatures (T_d, 5% weight loss temperature) of the polymers. The block copolymers exhibit two thermal degradation temperatures around 381 °C and 441 °C, which are attributed to the decomposition of P4VP and PF, respectively.[34,35] Fig. 2b illustrates the DSC curves of the PF-*b*-P4VP block copolymers at a heating rate of 5 °C min^{-1} under nitrogen atmosphere. The glass transition temperatures (T_g) of the synthesized PF macroinitiator and P4VP homopolymer (M_n = 20788 g mol^{-1}) are 84 °C and 147 °C, respectively. The T_g of PF_9-*b*-$P4VP_{22}$, PF_9-*b*-$P4VP_{92}$, and PF_9-*b*-$P4VP_{231}$ are 84 °C, 145 °C, and 147 °C, respectively, increasing with P4VP chain length.

Microphase separation of PF-*b*-P4VP

The TEM image, SAXS data of bulk samples and the AFM images of thin films for PF_9-*b*-$P4VP_{22}$ ($f_{P4VP} = 0.42$) are shown in

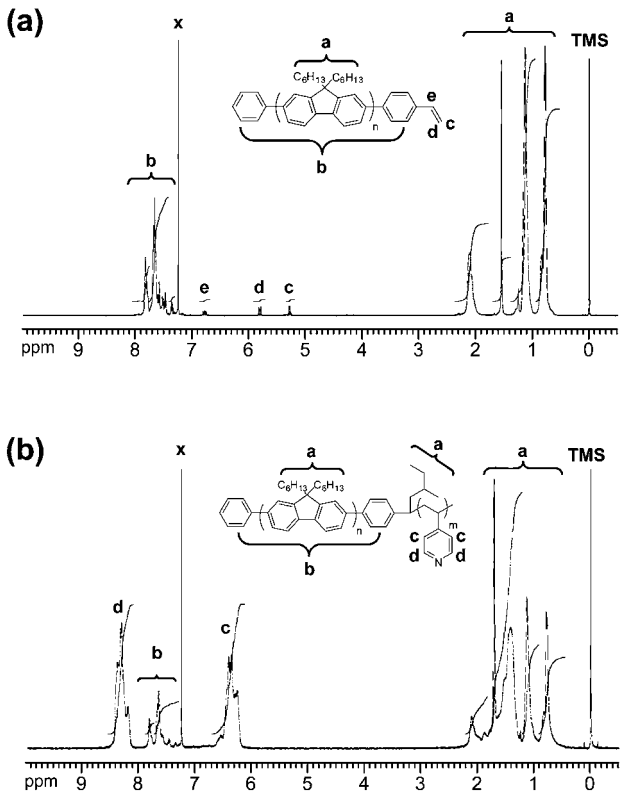

Fig. 1 ^{1}H NMR spectra of (a) PF_9 macroinitiator and (b) PF_9-*b*-$P4VP_{92}$ diblock copolymer.

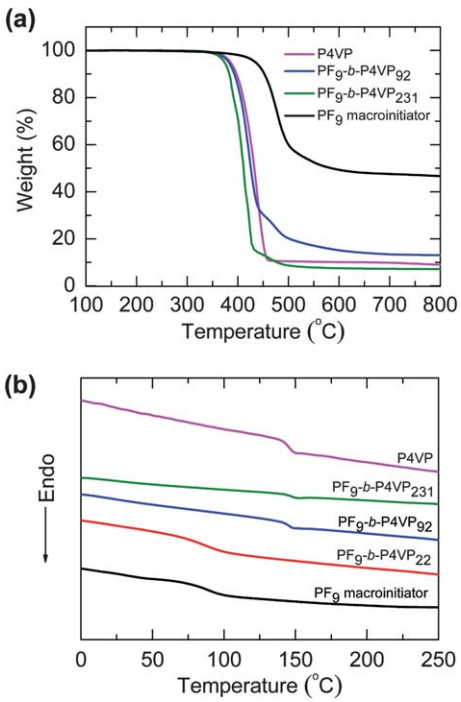

Fig. 2 (a) TGA and (b) DSC thermograms of PF_9 macroinitiator and PF-*b*-P4VP diblock copolymers.

Fig. 3. The TEM image (Fig. 3a), which was obtained using RuO_4 to stain the PF blocks, shows striped clusters distributed in homogeneous matrix. Since the two blocks of PF_9-*b*-$P4VP_{22}$ are approximately symmetric, the alternating stripes should be lamellar microdomains oriented normal to the section plane. In the wide plain regions, however, no structures are observed, indicating that microphase separation only occurs locally. A plausible explanation for this unusual phase behavior is that the lengths of PF and P4VP of this diblock copolymer are short, giving rise to a low χN value. This low χN of PF_9-*b*-$P4VP_{22}$ happens to locate around the border of isotropic and lamellar phases, *i.e.* in the weak segregation limit, resulting in a transitional morphology. Similar morphology has been reported in poly-(diethylhexyloxy-*p*-phenylenevinylene)-*b*-polystyrene rod-coil systems.[36,37] In the clusters, the lamellae are bended and discontinuous and have a varying spacing. The variation of the lamellar spacing also implies a weak segregation. The spacing of the lamellae estimated from the relatively regular regions in TEM image is ~20 nm. The low fraction of lamellar clusters and the lack of ordering in the clusters are reflected on the SAXS measurements where no distinct diffraction peak appears, as shown in Fig. 3b.

We now move on to the thin film morphology of PF_9-*b*-$P4VP_{22}$. In thin films, the interactions between substrate and polymers are involved in determining the microphase separation behaviors. Fig. 3c shows the AFM images of a thin film, ~79 nm in thickness, which reveals the coexistence of strips and flat surfaces. The morphologies are essentially the same whether films were thermal annealed at 150 °C or solvent annealed. The strips should be the lamellar structures oriented perpendicular the surface. In the flat regions, holes are observed, shown in the height image, and the depth of the holes is 20–25 nm. This depth is consistent with the spacing of lamellae obtained from TEM. In coil–coil block copolymer systems, such holes usually occur on the surface of thin films with lamellar microdomains parallel to the surface if film thicknesses and the natural spacing of lamellae are incommensurable.[38] We thus believe that the flat regions are formed by lamellae as well but their orientation is parallel to the surface.

Fig. 3d shows the AFM images of a very thin film (less than 18 nm), in which long fibrils are meandering through flat surfaces and two different widths of fibrils are observed. The width of thinner fibrils is ~20 nm and they should be a single lamella perpendicular to the surface. The thicker ones are ~35 nm in width and presumably formed by the stacking of two lamellae. Note that holes are formed on the flat region, ~6 nm in depth, implying a monolayer deposited on the substrate.[39] In the monolayer, the more hydrophilic P4VP blocks should adhere to the silicon substrate while the PF blocks are exposed to the air. Comparing Fig. 3c and 3d, the fraction of the perpendicular lamellae in thicker films is higher than that in thinner films. It is well known that the substrate-block copolymer interactions greatly affect the morphology of a thin layer close to the interface and if the substrate prefers to interact with one of the blocks, microdomains are generally forced to be parallel to the surface.[40] For a very thin film, the entire film is almost influenced by the preferential interaction between the substrate and P4VP, thereby forming mostly parallel lamellae; as film thickness is increased, the effect is gradually vanished away from the substrate and thus perpendicular lamellae are increasingly formed.[41]

The bulk and thin film morphologies of PF_9-*b*-$P4VP_{92}$ that has coil fraction increased to 0.76 are shown in Fig. 4. In the TEM image (Fig. 4a), where P4VP were stained with I_2, the PF blocks self-assemble into cylindrical microdomains and the cylinders are hexagonally packed, in contrast to the irregular packing of lamellae in PF_9-*b*-$P4VP_{22}$. SAXS data, shown in Fig. 4b, reveal a distinct first-order peak at $q^* = 0.031$ Å^{-1}, which corresponds to a d-spacing of 20.3 nm, and an obscure second-order peak at $q = \sqrt{3}\,q^*$. The ratio of $1{:}\sqrt{3}$ also suggests a hexagonal packing of cylinders. In the AFM images of a thin film, ~135 nm in thickness, the structure on the surface is hardly seen in the height image, shown in Fig. 4c, indicating that the surface is rather

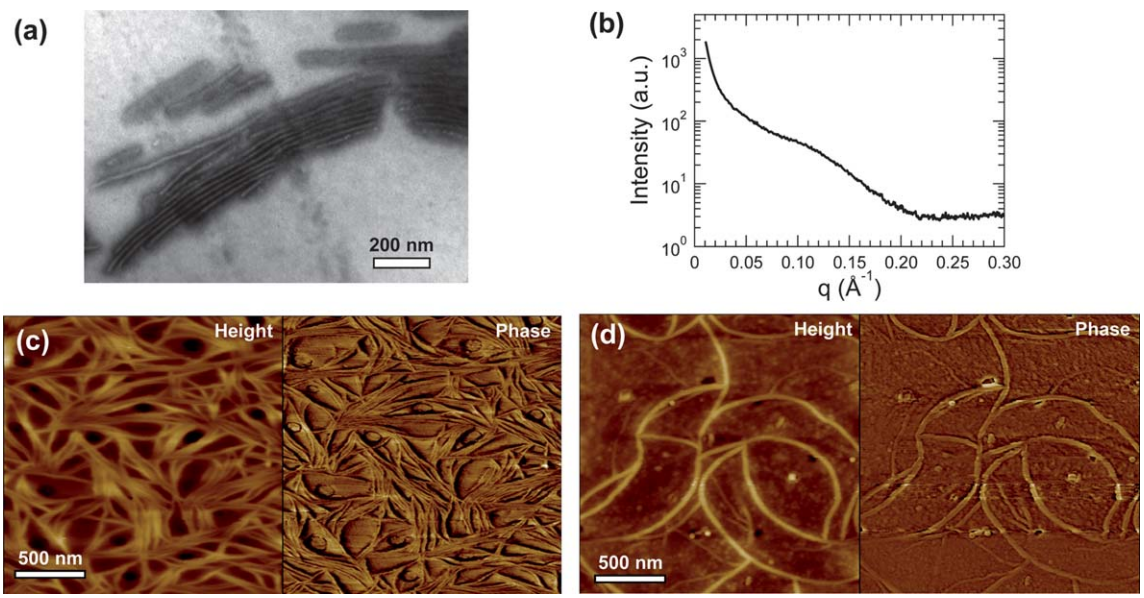

Fig. 3 Structure characterization of PF_9-*b*-$P4VP_{22}$: (a) TEM image and (b) SAXS curve for bulk samples. The TEM sample was stained with RuO_4. AFM images for (c) a thicker film ~79 nm in thickness and (d) a very thin film (less than 18 nm).

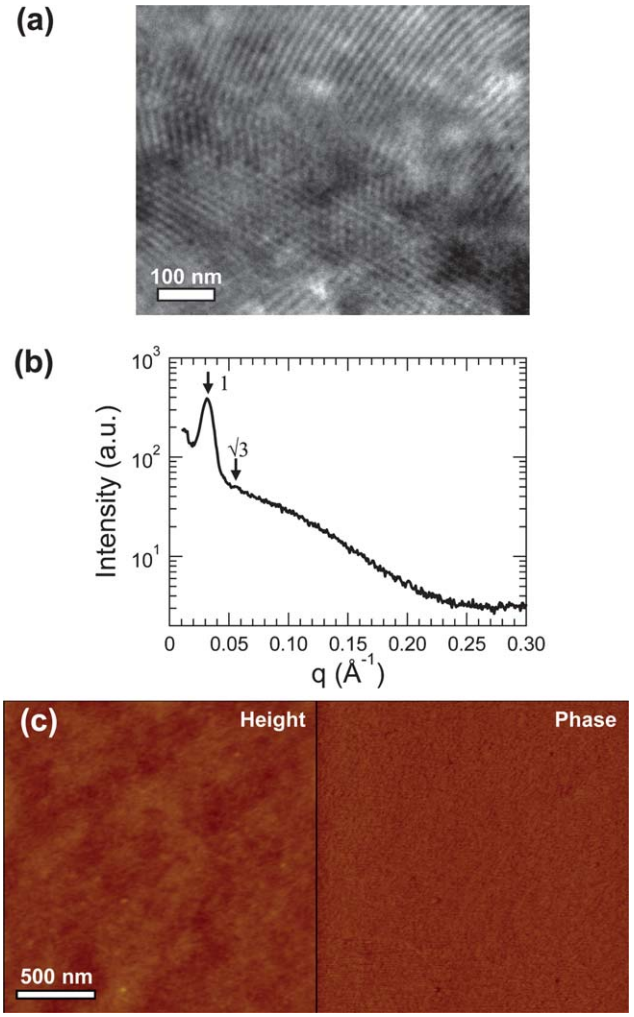

Fig. 4 Structure characterization of PF_9-*b*-$P4VP_{92}$: (a) TEM image and (b) SAXS curve for bulk samples. The TEM sample was stained with I_2. (c) AFM images for a thin film ~135 nm in thickness.

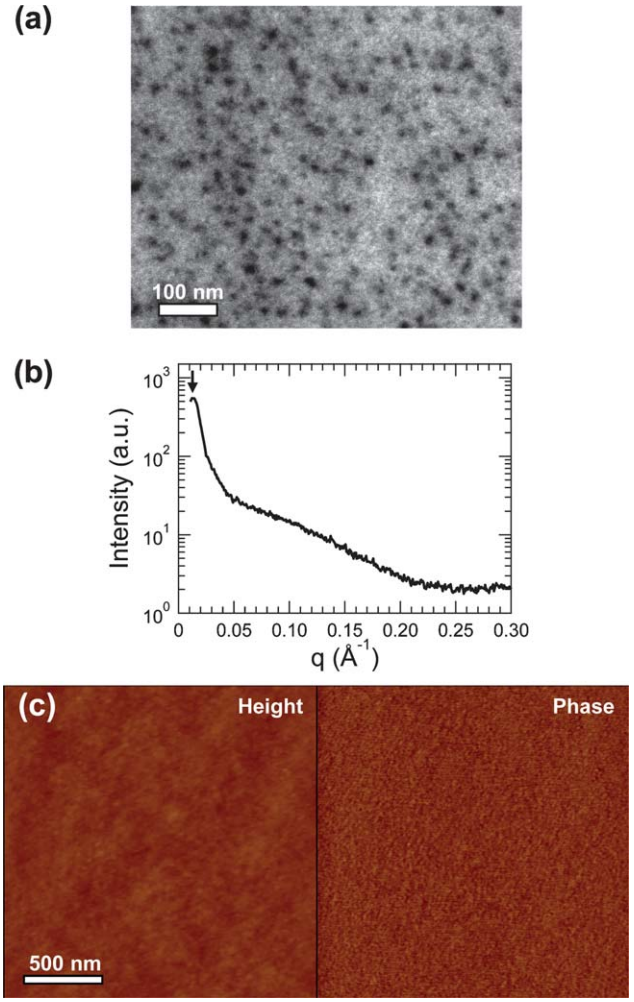

Fig. 5 Structure characterization of PF_9-*b*-$P4VP_{231}$: (a) TEM image and (b) SAXS curve for bulk samples. The TEM sample was stained with RuO_4. (c) AFM images for a thin film ~65 nm in thickness.

smooth, which is again different from the rough surface of PF_9-*b*-$P4VP_{22}$ thin films (Fig. 3c). The phase image shows no significant feature either. The barely distinguishable phase image is due to naturally low phase contrast between PF and P4VP blocks since the hardness and adhesion of PF and P4VP are comparable.

For the sample of PF_9-*b*-$P4VP_{231}$, the coil fraction further increased to 0.89, the PF blocks turn into spherical microdomains, as shown in the TEM image in Fig. 5a, where PF blocks were stained with RuO_4. In Fig. 5b, the SAXS data show a diffraction peak at $q = 0.014$ Å^{-1}, implying an average spacing of 44.9 nm between spheres. The higher-order peaks, however, are absent due to the lack of ordering. In thin films, the surface is quite smooth and the spherical microdomains could only be vaguely observed in the height and phase AFM images, shown in Fig. 5c. As the coil length increases, which relatively reduces the effects of π interaction and thus increases the mobility of polymer chains during annealing, the surface tends to become smoother to reduce the surface area and lower the surface free energy.

In addition to the PF_9-based rod-coil block copolymers, we have also synthesized copolymers with longer rod lengths, whose morphologies are presented in supplementary information. It appears that the transition of the PF-*b*-P4VP morphology, from lamella to cylinder to sphere, is dependent on the volume fractions of blocks, which has been found in some rod-coil systems.[29,42,43] This relationship has been well known for coil–coil block copolymers. The difference is that the packing of microdomains in PF-*b*-P4VP is not as ordered as that of coil–coil ones due to the strong π–π interaction and the steric interaction of PF rod-like chains.

Characterization and microphase separation of PF-*b*-P4VP(PDP)

PF-*b*-P4VP(PDP) supramolecules are prepared by hydrogen-bonding 3-pentadecylphenol (PDP) to the 4VP. The

Table 2 Characteristics of PF-*b*-P4VP(PDP) supramolecules

Sample	f_{comb}[a]	Morphology
PF_9-*b*-$P4VP_{22}(PDP)_1$	0.74	cylinder
PF_9-*b*-$P4VP_{92}(PDP)_1$	0.92	sphere
PF_9-*b*-$P4VP_{231}(PDP)_1$	0.97	sphere

[a] weight fraction of P4VP(PDP).

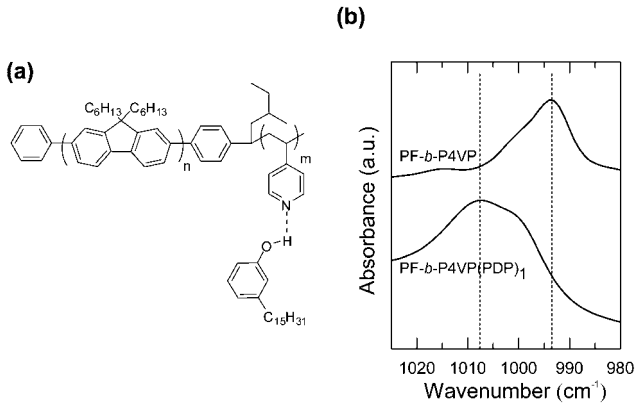

Fig. 6 (a) Schematic of PF-*b*-P4VP(PDP) supramolecule. (b) FT-IR spectra of PS-*b*-P4VP and PS-*b*-P4VP(PDP)$_1$.

characteristics of the samples are listed in Table 2. The chemical structure of the rod-comb PF-*b*-P4VP(PDP) supramolecule is illustrated in Fig. 6a. Fig. 6b shows the FT-IR spectra of a PF-*b*-P4VP(PDP)$_1$ thin film where the subscript denotes the molar ratio of PDP to 4VP. Free pyridine groups of PF-*b*-P4VP produce an absorption band at 993 cm^{-1}. Upon the incorporation of PDP, as seen in the spectrum of PF-*b*-P4VP(PDP)$_1$, this band shifts to a higher frequency ~1008 cm^{-1}. This is evidence that the pyridines are hydrogen-bonded with phenyl groups of PDP and the formation of the supramolecule PF-*b*-P4VP(PDP) is confirmed.

Fig. 7 shows the AFM images of supramolecular thin films. With the incorporation of PDP, the PF rich domains and P4VP(PDP) rich domains can be clearly distinguished in phase images. This is because the soft PDPs enhance the contrast of hardness and adhesion between the PF and the P4VP(PDP) blocks. As shown in Fig. 7a, the morphology of PF$_9$-*b*-P4VP$_{22}$(PDP)$_1$ (f_{comb} = 0.74) are entirely different from that of pure PF$_9$-*b*-P4VP$_{22}$. The addition of PDP transforms the lamellar structures of PF$_9$-*b*-P4VP$_{22}$ (Fig. 3c) into straight but discontinuous cylinders formed by PF blocks. Different from regular hexagonally-packed cylindrical microdomains found in coil–coil block copolymer-based supramolecules,[27,44] the PF cylinders are randomly embedded in P4VP(PDP) matrix. The SAXS data of a bulk PF$_9$-*b*-P4VP$_{22}$(PDP)$_1$ sample are shown in Fig. 8. A hump at $q \approx 0.055$ Å^{-1} indicates the distance between cylinders is about 11.4 nm.

In the thin films cast from PF$_9$-*b*-P4VP$_{92}$(PDP)$_1$ (f_{comb} = 0.92), the PF blocks form mostly spherical microdomains along with a few short curly cylindrical ones in P4VP(PDP) matrix, shown in Fig. 7b, which is transformed from the hexagonally-packed cylindrical microdomains found in pure PF$_9$-*b*-P4VP$_{92}$ (Fig. 4c). The morphology of this supramolecule should be in the transitional state between cylindrical and spherical phases. Further increasing P4VP length, as demonstrated in PF$_9$-*b*-P4VP$_{231}$(PDP)$_1$ thin films, though the fraction of P4VP(PDP) is as high as 0.97, phase-separations between PF and P4VP(PDP) are still observed and the PF microdomains remain spherical, shown in Fig. 7c. The first order peaks of SAXS data for PF$_9$-*b*-P4VP$_{92}$(PDP)$_1$ and PF$_9$-*b*-P4VP$_{231}$(PDP)$_1$ bulk samples shown in Fig. 8 are at q = 0.042 and 0.018 Å^{-1}, respectively, corresponding to center-to-center distances between spheres of 14.9 and 34.9 nm.

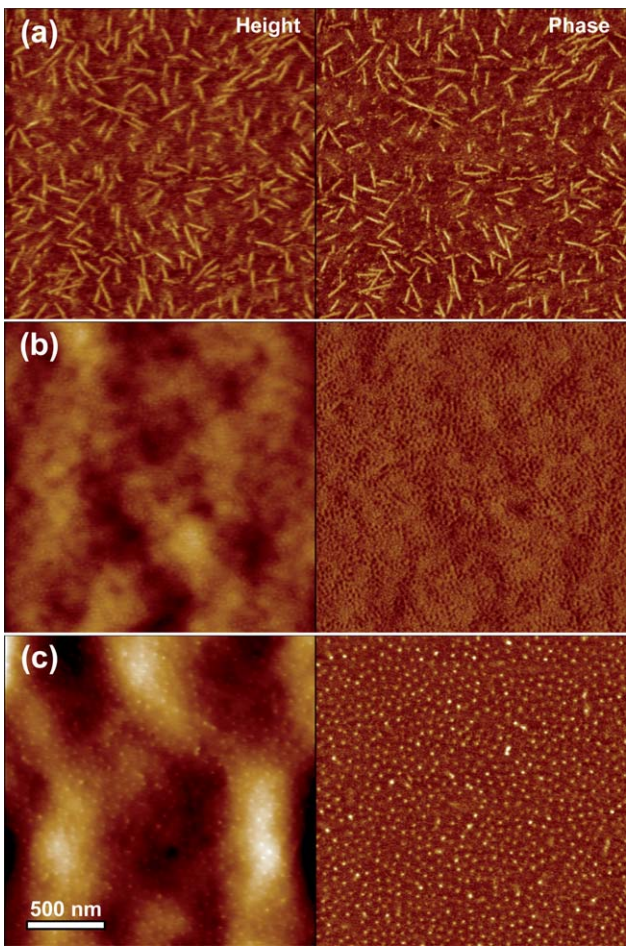

Fig. 7 AFM images for (a) a PF$_9$-*b*-P4VP$_{22}$(PDP)$_1$ thin film, thickness = 119 nm, (b) a PF$_9$-*b*-P4VP$_{92}$(PDP)$_1$ thin film, film thickness = 327 nm and (c) a PF$_9$-*b*-P4VP$_{231}$(PDP)$_1$ thin film, film thickness = 117 nm.

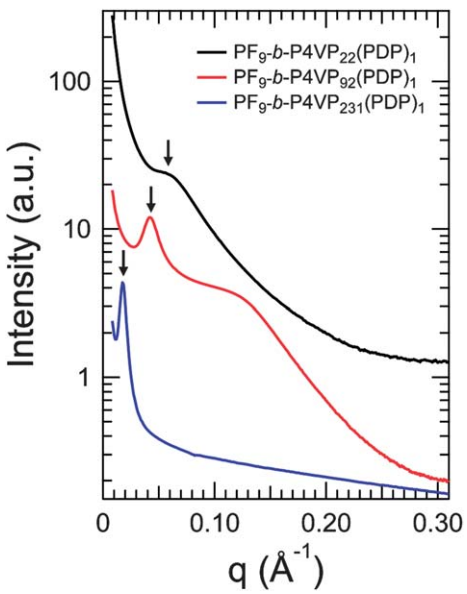

Fig. 8 SAXS data of PF-*b*-P4VP(PDP)$_1$ bulk samples.

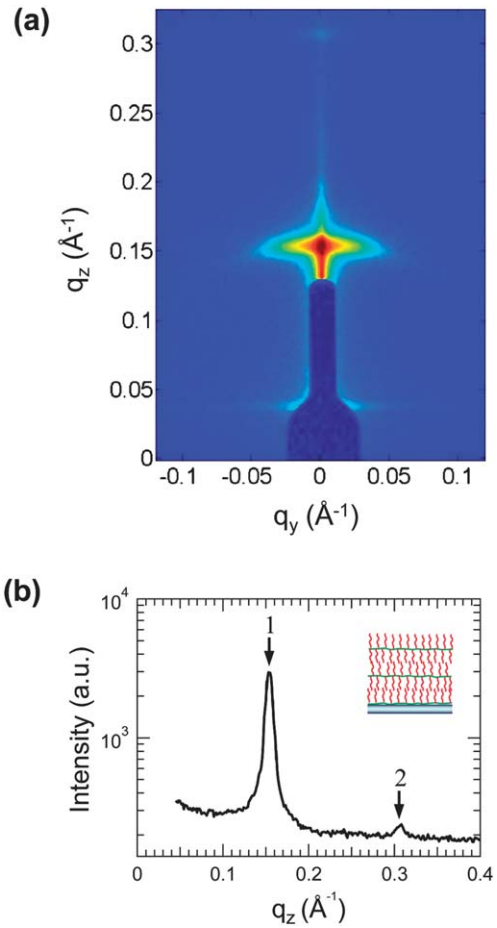

Fig. 9 (a) GISAXS pattern of a ~100 nm PF_9-*b*-$P4VP_{231}(PDP)_1$ thin film at an incident angle of 0.2°. (b) The q_z scan at $q_y = 0.015$ Å^{-1}, showing the P4VP(PDP) lamellae with a spacing of 4.1 nm are oriented parallel to the surface.

Fig. 9a shows the GISAXS pattern of a PF_9-*b*-$P4VP_{231}(PDP)_1$ thin film, ~100 nm in thickness, where the diffraction spots only appear along q_z axis. The q_z scan at $q_y = 0.015$ Å^{-1}, plotted in Fig. 9b, shows the first-order peak at $q_z = 0.153$ Å^{-1} and the second-order one at $q_z = 0.308$ Å^{-1}, corresponding to a spacing of ~4.1 nm, which is due to the ordering of the lamellae formed by the P4VP(PDP) comb blocks oriented parallel to the surface. The alignment of P4VP(PDP) lamellae is schemed in the inset of Fig. 9b. Since P4VP blocks are more hydrophilic and preferentially interacts with silicon oxide, the hydrophobic alkyl tails of PDPs are precluded from P4VP(PDP)/substrate interfaces. Also, the alkyl tails of PDPs tend to be exposed to air and thus the P4VP(PDP) lamellae are stacked parallel to the surface. Such structure has been found in other supramolecular systems.[44,45] Note that the diffraction peak of the lamellae is absent in the SAXS data of bulk samples shown in Fig. 8. The substrate-P4VP interaction force should play an important role in regulating the lamellae. Furthermore, we didn't observe the parallel lamellae in the PF_9-*b*-$P4VP_{22}(PDP)_{1.0}$ and PF_9-*b*-$P4VP_{92}(PDP)_1$ thin film, implying that a larger fraction of rod PF blocks may prohibit P4VP(PDP) comb blocks from regular stacking even though the interfacial effect exists.

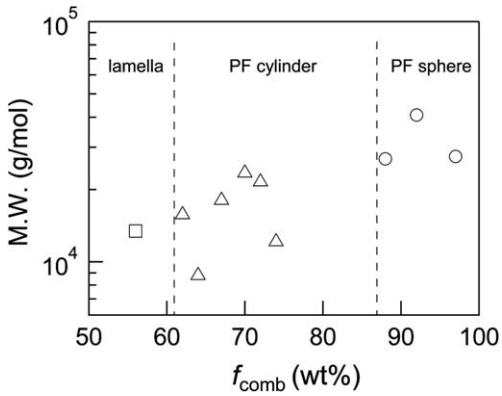

Fig. 10 Morphology diagram of PF-*b*-P4VP(PDP) as a function of the weight fraction of the comb-like block P4VP(PDP) (f_{comb}) at room temperature. M.W. is the total molecular weight of the PF-*b*-P4VP(PDP) supramolecules. The morphologies of most compositions are shown in supplementary information.

The morphologies of more PF-*b*-P4VP(PDP) supramolecules with different fractions of blocks and PDP/4VP ratios are presented in supplementary information. The phase behaviors of all the characterized samples are summarized in Fig. 10. It is clear that PDPs can associate with P4VP blocks and therefore increase the volume fraction of P4VP(PDP), which in turn, transforms the PF microdomains from lamella to cylinder or from cylinder to sphere. In other word, the morphology of rod-coil block copolymers can be tailored by supramolecular strategies. This effect has been seen in coil-coil block copolymer-based supramolecules. However, in rod-coil systems, the packing of microdomains are governed by the π-stacking of rod blocks. The arrangement of microdomains is thus less ordered and the orientation control in thin films is not as efficient as in coil-coil analogues.[25–28]

4. Conclusions

This study has demonstrated that the supramolecular strategy is a facile way to manipulate the morphology of rod-coil block copolymers. The strategy involves the incorporation of small molecules *via* hydrogen bonding into the coil blocks to form rod-comb supramolecules. We have synthesized a series of new fluorene-based block copolymers (PF-*b*-P4VP) with different coil chain lengths through Suzuki coupling reaction and living anionic polymerization and we show the feasibility of this strategy by incorporating PDP into P4VP blocks. The morphology can indeed be transformed from lamellar to cylinder or from cylinder to spherical upon the addition of PDP. We also show that the π–π interaction is a crucial factor that governs the microphase separation in supramolecular assemblies.

Acknowledgements

This work was financially supported by the Taiwan National Science Council (NSC 99-2923-E-002-003). We acknowledge NSRRC, Taiwan for facilitating the SAXS and GISAXS experiments performed as part of this work and Dr U-Ser Jeng and Dr Chun-Jen Su of NSRRC for the assistance in scattering experiments. We also thank Mr. Nao Xiao at Hokkaido University for the assistance in GPC experiments.

References

1 M. Lee, B. K. Cho and W. C. Zin, *Chem. Rev.*, 2001, **101**, 3869–3892.
2 P. Leclere, E. Hennebicq, A. Calderone, P. Brocorens, A. C. Grimsdale, K. Mullen, J. L. Bredas and R. Lazzaroni, *Prog. Polym. Sci.*, 2003, **28**, 55–81.
3 B. D. Olsen and R. A. Segalman, *Mater. Sci. Eng., R*, 2008, **62**, 37–66.
4 S. A. Jenekhe and X. L. Chen, *Science*, 1998, **279**, 1903–1907.
5 J. H. Kim, M. S. Rahman, J. S. Lee and J. W. Park, *J. Am. Chem. Soc.*, 2007, **129**, 7756–7757.
6 J. T. Chen, E. L. Thomas, C. K. Ober and G. P. Mao, *Science*, 1996, **273**, 343–346.
7 J. Cornelissen, M. Fischer, N. Sommerdijk and R. J. M. Nolte, *Science*, 1998, **280**, 1427–1430.
8 K. K. Tenneti, X. F. Chen, C. Y. Li, Y. F. Tu, X. H. Wan, Q. F. Zhou, I. Sics and B. S. Hsiao, *J. Am. Chem. Soc.*, 2005, **127**, 15481–15490.
9 B. D. Olsen, M. Shah, V. Ganesan and R. A. Segalman, *Macromolecules*, 2008, **41**, 6809–6817.
10 A. J. Berresheim, M. Muller and K. Mullen, *Chem. Rev.*, 1999, **99**, 1747–1785.
11 R. A. Segalman, B. McCulloch, S. Kirmayer and J. J. Urban, *Macromolecules*, 2009, **42**, 9205–9216.
12 D. Neher, *Macromol. Rapid Commun.*, 2001, **22**, 1366–1385.
13 U. Scherf and E. J. W. List, *Adv. Mater.*, 2002, **14**, 477–487.
14 L. L. Chua, J. Zaumseil, J. F. Chang, E. C. W. Ou, P. K. H. Ho, H. Sirringhaus and R. H. Friend, *Nature*, 2005, **434**, 194–199.
15 S. Lu, T. X. Liu, L. Ke, D. G. Ma, S. J. Chua and W. Huang, *Macromolecules*, 2005, **38**, 8494–8502.
16 Y. C. Tung, W. C. Wu and W. C. Chen, *Macromol. Rapid Commun.*, 2006, **27**, 1838–1844.
17 S. T. Lin, K. Fuchise, Y. G. Chen, R. Sakai, T. Satoh, T. Kakuchi and W. C. Chen, *Soft Matter*, 2009, **5**, 3761–3770.
18 C. L. Chochos, P. K. Tsolakis, V. G. Gregoriou and J. K. Kallitsis, *Macromolecules*, 2004, **37**, 2502–2510.
19 P. Leclere, M. Surin, P. Jonkheijm, O. Henze, A. Schenning, F. Biscarini, A. C. Grimsdale, W. J. Feast, E. W. Meijer, K. Mullen, J. L. Bredas and R. Lazzaroni, *Eur. Polym. J.*, 2004, **40**, 885–892.
20 M. Surin, D. Marsitzky, A. C. Grimsdale, K. Mullen, R. Lazzaroni and P. Leclere, *Adv. Funct. Mater.*, 2004, **14**, 708–715.
21 M. Muthukumar, C. K. Ober and E. L. Thomas, *Science*, 1997, **277**, 1225–1232.
22 G. ten Brinke, J. Ruokolainen and O. Ikkala, in *Hydrogen Bonded Polymers*, Springer-Verlag Berlin, Berlin, 2007, vol. 207, pp. 113–177.
23 M. R. Hammond and R. Mezzenga, *Soft Matter*, 2008, **4**, 952–961.
24 O. Ikkala and G. ten Brinke, *Chem. Commun.*, 2004, 2131–2137.
25 I. Tokarev, R. Krenek, Y. Burkov, D. Schmeisser, A. Sidorenko, S. Minko and M. Stamm, *Macromolecules*, 2005, **38**, 507–516.
26 K. Albrecht, A. Mourran, X. Zhu, T. Markkula, J. Groll, U. Beginn, W. H. deJeu and M. Moeller, *Macromolecules*, 2008, **41**, 1728–1738.
27 S. H. Tung, N. C. Kalarickal, J. W. Mays and T. Xu, *Macromolecules*, 2008, **41**, 6453–6462.
28 J. W. Lee, C. Lee, S. Y. Choi and S. H. Kim, *Macromolecules*, 2010, **43**, 442–447.
29 N. Sary, L. Rubatat, C. Brochon, G. Hadziioannou, J. Ruokolainen and R. Mezzenga, *Macromolecules*, 2007, **40**, 6990–6997.
30 N. Sary, F. Richard, C. Brochon, N. Leclerc, P. Leveque, J. N. Audinot, S. Berson, T. Heiser, G. Hadziioannou and R. Mezzenga, *Adv. Mater.*, 2010, **22**, 763–768.
31 D. Marsitzky, M. Klapper and K. Mullen, *Macromolecules*, 1999, **32**, 8685–8688.
32 C. H. Lin, Y. C. Tung, J. Ruokolainen, R. Mezzenga and W. C. Chen, *Macromolecules*, 2008, **41**, 8759–8769.
33 U. S. Jeng, C. H. Su, C. J. Su, K. F. Liao, W. T. Chuang, Y. H. Lai, J. W. Chang, Y. J. Chen, Y. S. Huang, M. T. Lee, K. L. Yu, J. M. Lin, D. G. Liu, C. F. Chang, C. Y. Liu, C. H. Chang and K. S. Liang, *J. Appl. Crystallogr.*, 2010, **43**, 110–121.
34 C. F. Huang, S. W. Kuo, J. K. Chen and F. C. Chang, *J. Polym. Res.*, 2005, **12**, 449–456.
35 W. C. Wu, C. L. Liu and W. C. Chen, *Polymer*, 2006, **47**, 527–538.
36 N. Sary, C. Brochon, G. Hadziioannou and R. Mezzenga, *Eur. Phys. J. E*, 2007, **24**, 379–384.
37 N. Sary, R. Mezzenga, C. Brochon, G. Hadziioannou and J. Ruokolainen, *Macromolecules*, 2007, **40**, 3277–3286.
38 P. F. Green and R. Limary, *Adv. Colloid Interface Sci.*, 2001, **94**, 53–81.
39 J. H. Kim, M. S. Rahman, J. S. Lee and J. W. Park, *Macromolecules*, 2008, **41**, 3181–3189.
40 E. Huang, L. Rockford, T. P. Russell and C. J. Hawker, *Nature*, 1998, **395**, 757–758.
41 B. D. Olsen, X. F. Li, J. Wang and R. A. Segalman, *Macromolecules*, 2007, **40**, 3287–3295.
42 C. A. Dai, W. C. Yen, Y. H. Lee, C. C. Ho and W. F. Su, *J. Am. Chem. Soc.*, 2007, **129**, 11036–11038.
43 C. C. Ho, Y. H. Lee, C. A. Dai, R. A. Segalman and W. F. Su, *Macromolecules*, 2009, **42**, 4208–4219.
44 W. van Zoelen, E. Polushkin and G. ten Brinke, *Macromolecules*, 2008, **41**, 8807–8814.
45 B. J. Rancatore, C. E. Mauldin, S. H. Tung, C. Wang, A. Hexemer, J. Strzalka, J. M. J. Frechet and T. Xu, *ACS Nano*, 2010, **4**, 2721–2729.

